A fast model predictive control allocation of distributed drive electric vehicles for tire slip energy saving with stability constraints

GUO, Ningyuan, ZHANG, Xudong, ZOU, Yuan, LENZO, Basilio <http://orcid.org/0000-0002-8520-7953>, ZHANG, Tao and GÖHLICH, Dietmar

Published version

GUO, Ningyuan, ZHANG, Xudong, ZOU, Yuan, LENZO, Basilio, ZHANG, Tao and GÖHLICH, Dietmar (2020). A fast model predictive control allocation of distributed drive electric vehicles for tire slip energy saving with stability constraints. Control Engineering Practice, 102, p. 104554.

A Fast Model Predictive Control Allocation of Distributed Drive Electric Vehicles for Tire Slip Energy Saving with Stability Constraints

Ningyuan Guo[1], Xudong Zhang[1]*, Yuan Zou[1], Basilio Lenzo[2], Tao Zhang[1], and Dietmar Göhlich[3]
[1]National Engineering Laboratory for Electric Vehicles, School of Mechanical Engineering, and Collaborative Innovation Center of Electric Vehicles in Beijing, Beijing Institute of Technology, Beijing, China
[2]Department of Engineering and Mathematics, Sheffield Hallam University, Sheffield, United Kingdom
[3]Product Development Methods and Mechatronics, Technical University of Berlin, Berlin, Germany
E-mails: gny123@qq.com; xudong.zhang@bit.edu.cn; zouyuanbit@vip.163.com; basilio.lenzo@shu.ac.uk; ztao1208@126.com; dietmar.goehlich@tu-berlin.de

Abstract: This paper proposes a fast model predictive control allocation (MPCA) approach to minimize the tire slip power loss on contact patches for distributed drive electric vehicles (DDEV). In this strategy, two assumptions are set up from a practical focus: 1) the vehicle acceleration and yaw rate are measureable by global position system (GPS)/ inertial navigation system (INS) and inertial measurement unit (IMU), respectively; 2) the longitudinal velocity, road adhesion factor, and vehicle yaw rate are arranged to be "already known" by advanced estimators. For the strategy design, a CarSim-embedded driver model and a linear quadratic regulator (LQR) based direct yaw moment controller, are respectively applied to calculate the desired longitudinal traction and yaw moment as a virtual input first. Then, a MPCA method is proposed to reasonably distribute the virtual input among four in-wheel motors in order to optimize the tire slip power loss and vehicle stability performance. To accurately characterize tire slip power loss in MPCA, a tire slip estimator is established for tire slip information acquirement. Moreover, addressing on the heavily computational challenge in MPCA, a modified continuation/generalized minimal residual (C/GMRES) algorithm is employed. Since the traditional C/GMRES algorithm cannot directly solve the inequality constraint problem, the barrier functions are applied for transforming the inequality constraints to equivalent cost. According to Pontryagin's minimum principle (PMP) conditions, the existence and uniqueness for solution of the modified C/GMRES algorithm are strictly proved. Subsequently, a Karush-Kuhn-Tucker (KKT) condition based approach is developed to fast gain the optimally initial solution in C/GMRES algorithm for extending application. Finally, numerical simulation validations are implemented and demonstrate that the proposed MPCA can ensure the compatibility between the tire slip power loss reduction and vehicle stability in a computationally efficient way.

Key words: continuation/generalized minimal residual algorithm, distributed drive electric vehicle, fast model predictive control allocation, tire slip power loss, vehicle stability.

I. INTRODUCTION

Electric vehicles (EV) have become one of promising solutions in future transportation electrification, owing to its advantages of none exhaust emission, fast drive response, high energy utilizing ratio and so forth (Zhang et al., 2019). For EVs, one highlighted configuration is the distributed drive electric vehicles (DDEV). Unlike traditional central drive EVs, the in-wheel motor (IWM) assembles in each wheel of DDEV and acts as the power output unit, providing more control flexibilities to improve vehicle dynamic performance. This kind of control system is called over-actuation; however, such feature also brings the control redundancy thus entailing control difficulties in DDEVs. To handle it, control allocation (CA) is a widely-used and effective approach, which aims to simultaneously satisfy the virtual motion control targets from upper-level motion control and allocate lower-level IWMs' torques for desirable targets (Hu et al., 2019a).

Various CA objectives are put forward in literature, mainly including the tire slip rate, the tire workload usage, the motor's power loss, and the tire slip power loss. Ref. (Yoshimura and Fujimoto, 2012) designs a CA method to minimize the tire slip rate for vehicle stabilization. Similarly for the vehicle stability, several researches (Zhang and Göhlich, 2017, Yue et al., 2018) employ the tire workload usage minimization as objective, which aims to maximize the attachment margin of tires and indirectly keep the tire force far away from its nonlinear saturation region. In order to extend the drive mileage, CAs in reduction of motors' power loss are also proposed. Ref. (Chen and Wang, 2014) develops a fast energy optimization based CA approach that can arrange the IWMs' operation points in higher efficiency region by analytical calculation under longitudinal drive cases.

Although above researches are successful, they can only consider the single objective, namely the vehicle stability or vehicle energy efficiency. For the adaptive capacity of complicated and changeable drive cycles, the compatibility between vehicle energy efficiency and vehicle stability performance is required. Hence, a few researchers gradually focus on the CA of tire slip power loss minimization (Zhao et al., 2019, Kobayashi et al., 2017). Its primary target is to reduce the tire slip power loss on contact patches for improving the all-electric range

of vehicles, by which the tire heating dissipation is declined and the tire lifetime can be extended to some extent. Additionally, since the tire slip rate couples with tire slip power loss and vehicle dynamics, the CAs for tire slip power loss minimization is able to simultaneously implement the desirable energy efficiency and vehicle stabilization. By comprehensively analytic derivation, Ref. (Filippis et al., 2018) proposes a sub-optimal CA strategy in reducing IWMs' energy consumption and tire slip power loss. However, it directly takes the tire forces to evaluate tire slip power loss, which brings a relative deviation between real and estimated values and thus results in undesirable control effect. In (Suzuki et al., 2014), a more reasonable expression of tire slip power loss is designed. The tire brush model is adopted to estimate tire slip force and slip rate, and a pseudoinverse-based CA method is delegated to satisfy the vehicle stability and reduce the tire slip power loss simultaneously. To further enhance the estimation accuracy of tire dynamics, Ref. (Zhao et al., 2019) adopts the UniTire model for online estimation of tire slip power loss. However, applying the complicated semi-empirical model in tire dynamics estimation leads to the tedious labor burden in parameter tuning.

In the field of CA approaches, the general ones are rule-based allocation, daisy-chain allocation, redistributed pseudo-inverse allocation, and optimization-based allocation. In (Park et al., 2020), the daisy-chain CA method is developed to successively set up the drive forces of wheels under the descending order of contribution if the first wheel reaches its adhesion limit. This method, however, leads to the extremely uneven torque distribution of IWMs' drive forces, which is inconsistent with sufficient application of each IWM for expected effects. Compared with above methods, the optimization based CAs can quantitatively evaluate the control effects and impose the equality/inequality constraints with ease, thereby increasingly being employed in torque distribution of DDEVs. In (Guo et al., 2020a), a method based on Karush-Kuhn-Tucker (KKT) conditions is adopted to fast optimize the tire workload usages of IWMs, showing the desirable effects and guaranteed stability limits.

To further improve control effects, model predictive control (MPC) based CA (Johansen and Fossen, 2013), i.e., model predictive control allocation (MPCA), is gradually applied in IWM's torque distribution of DDEVs. Unlike the CAs that only focus on current states, MPCAs are able to optimize the future system dynamics of a short-term predictive horizon for more desirable control effects (Englert and Graichen, 2020). In (Zhao et al., 2015), to hold the vehicle stability, the optimization problem of MPCA is established, considering a series of constraints,

such as IWMs' output limits, tire slip rate limits and so forth. Results yield that the MPCA method can conduct superior transition performance and smoother control command compared with the CAs that only focus on current states. That said, it is noteworthy that the online optimization of MPCA is not a facile task in practical implementation due to its huge computing burden. In (Yuan et al., 2016), a holistic MPCA is proposed with various safety constraints of DDEV. To validate its feasibility, the hardware-in-the-loop experiment is carried out by particle swarm optimization (PSO) algorithm under field programmable gate array (FPGA) chip. Thanks to the parallel calculation capacity of PSO and FPGA, the proposed MPCA is verified to be real-time applicable; nevertheless, the wider application of MPCA is still limited because of the expensive FPGA chip cost.

To fill above gaps, this paper proposes a fast MPCA focusing on the compatibility between the tire slip power loss and the vehicle stability. To this end, a hierarchical control framework is developed under the following assumptions: 1) from a practical focus, the vehicle acceleration and yaw rate are assumed to be measured by global position system (GPS)/ inertial navigation system (INS) (Hu et al., 2019c) and inertial measurement unit (IMU) (Lenzo et al., 2020), respectively; 2) the longitudinal velocity, road adhesion factor, and vehicle yaw rate are assumed to be "already known" by advanced estimators (Guo et al., 2018, Qin et al., 2018) to avoid distracting readers' focus. In upper level of control framework, a CarSim-embedded driver model is adopted to generate the front wheels' steering angle and longitudinal traction demands. Since the addressed study emphasis is the fast MPCA, the simple but effective approach, linear quadratic regulator (LQR), is applied for lateral motion control to gain the appropriate external yaw moment. A tire slip estimator is established for tire slip information acquirement. Given the external yaw moment and tire slip information, the MPCA controller is designed in the lower level for torque allocation. To migrate the computational burden, the continuation/generalized minimal residual (C/GMRES) algorithm is applied in MPCA. To fit the application of C/GMRES algorithm, the barrier functions are adopted to equivalently transform the inequality constrained problem as an unconstrained one, and the existence and uniqueness for solution is proved by the optimality conditions of Pontryagin's minimum principle (PMP). Furthermore, a KKT condition based approach is proposed to fast obtain the optimally initial solution in C/GMRES algorithm for expected optimization convergence. To sum up, the main contributions of this paper are listed below.

First, the MPCA control problem of torque allocation is properly and systematically established, considering the tire slip energy-saving effect and vehicle stability guarantee.

Second, to mitigate the heavy computational burden in MPCA, the C/GMRES algorithm is adopted and modified for fast optimization, yielding the applicable control effects and the real-time calculation efficiency for practical application.

Third, for proposed C/GMRES method, the sufficiency that solution is existent and exclusive, is strictly proved according to PMP optimality conditions.

Fourth, the tire slip information is online gained by the proposed estimation method and integrated into the proposed MPCA. Hence the tire model is not required in control-oriented model, and the optimization complexity of MPCA can be decreased.

The rest of this paper is organized as follows. Section II introduces the two degree-of-freedom (DOF) vehicle model and the tire slip rate update model. The proposed control framework, including yaw motion control, tire slip information estimation and MPCA, is elaborated in Section III. The validations of proposed MPCA method are demonstrated with in-depth analysis in Section IV, followed by the main conclusions in Section V.

II. Control-oriented Model Formulation

2.1. Two Degree-of-freedom Vehicle Model

The two DOF vehicle model is adopted in this paper, as the schematic depicted in Fig. 1, whose expression is presented (Hu et al., 2019b):

$$\dot{x}_t = A_t x_t + B_t u_t + D_t w_t \tag{1}$$

and

$$A_t = \begin{bmatrix} -\dfrac{2(C_f + C_r)}{mv_x} & -\dfrac{2(l_a C_f - l_b C_r)}{mv_x{}^2} - 1 \\ -\dfrac{2(l_a C_f - l_b C_r)}{I_z} & -\dfrac{2(l_a{}^2 C_f + l_b{}^2 C_r)}{I_z v_x} \end{bmatrix}, B_t = \begin{bmatrix} 0 \\ \dfrac{1}{I_z} \end{bmatrix}, D_t = \begin{bmatrix} \dfrac{2C_f}{mv_x} \\ \dfrac{2l_a C_f}{I_z} \end{bmatrix} \tag{2}$$

where $x_t = [\beta \quad \gamma]^T$ is the state variable, and $u_t = \Delta M$ is the control variable. $w_t = \delta$ is the external disturbance. β and γ denote the vehicle sideslip angle and the yaw rate, respectively. ΔM denotes the external yaw moment, and

δ is the front wheels' steering angle. C_f and C_r are the tire cornering stiffness of vehicle front and rear axles, respectively. l_a and l_b represent the distance from center-of-gravity (CoG) to front and rear axles, respectively. m and v_x are the vehicle mass and longitudinal velocity, respectively. I_z is the vehicle yaw inertia.

C_f and C_r are mainly influenced by tire vertical loads and road adhesion factor, which are expressed as (Ma et al., 2019),

$$\begin{cases} C_f = \mu C_{f0} \dfrac{F_{zf}}{F_{zf0}} \\ C_r = \mu C_{r0} \dfrac{F_{zr}}{F_{zr0}} \end{cases} \tag{3}$$

where μ is the road adhesion factor; C_{f0} and C_{r0} are the nominal cornering stiffness of front and rear tires, respectively; F_{zf0} and F_{zr0} are the nominally vertical load of the front and rear tires, respectively. F_{zf} and F_{zr} are the varying vertical load of front and rear tires, respectively. They can be expressed (Rajamani, 2006):

$$\begin{cases} F_{zf} = \dfrac{mgl_b - ma_x h_{cg}}{2(l_a + l_b)} \\ F_{zr} = \dfrac{mgl_b + ma_x h_{cg}}{2(l_a + l_b)} \end{cases} \tag{4}$$

where a_x is the longitudinal acceleration measured by GPS/ INS (Hu et al., 2019c), and h_{cg} is the height of vehicle CoG.

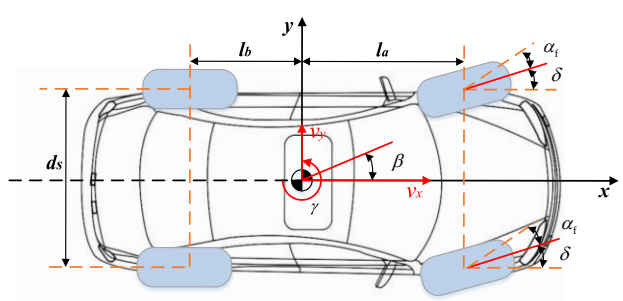

Fig. 1. Schematic of linear two DOF vehicle model.

2.2. Tire Slip Rate Model

Without the consideration of braking force compensation, the wheel rotational dynamics can be presented as,

$$J_s \dot{w}_i = T_i - r_w F_{xi} \tag{5}$$

where J_s is the wheel rotational inertia. w_i and $\dot{w}_i$ are the rotational speed and acceleration for the i th wheel, where subscript $i = 1,2,3,4$ denote the left-front, right-front, left-rear and right-rear, respectively and hereinafter. T_i is the output torque of the i th IWM, and r_w is the effective radius of wheel. F_{xi} is the longitudinal force of the i th tire. The tire longitudinal slip rate (Pomponi et al., 2018) is defined as,

$$\kappa_i = \frac{w_i r_w - v_{xi}}{v_{xi}} \tag{6}$$

where v_{xi} represents the longitudinal velocity of the i th wheel's center. Taking the slip rate derivative with respect to time, there is

$$\begin{aligned} \dot{\kappa}_i &= \frac{(\dot{w}_i r_w - \dot{v}_{xi}) v_{xi} - \dot{v}_{xi}(w_i r_w - v_{xi})}{{v_{xi}}^2} \\ &= \frac{\dot{w}_i r_w v_{xi} - w_{ij} r_w \dot{v}_{xi}}{{v_{xi}}^2} \end{aligned} \tag{7}$$

By Eq. (6), Eq. (7) can be rewritten as,

$$\dot{\kappa}_i = \frac{\dot{w}_i}{w_i}(\kappa_i + 1) - \frac{\dot{v}_{xi}}{w_i r_w}(\kappa_i + 1)^2 \tag{8}$$

Substituting $\dot{w}_i$ in Eq. (8) with Eq. (5) and defining $F_{xi} = C_{xi}\kappa_i$, it yields

$$\dot{\kappa}_i = \frac{T_i - r_w C_{xi}\kappa_i}{J w_i}(\kappa_i + 1) - \frac{a_{xi}}{w_i r_w}(\kappa_i + 1)^2 \tag{9}$$

where C_{xi} is the longitudinal slip stiffness of tire. $a_{xi} = \dot{v}_{xi}$ is the longitudinal acceleration of tire center. Based on Eq. (9), the state update function of tire slip rate is presented:

$$\begin{cases} \dot{x} = f(x,u) \\ y = C_d x \end{cases} \tag{10}$$

where $x = [\kappa_1, \kappa_2, \kappa_3, \kappa_4]^T$ is the system state vector, and $u = [T_1, T_2, T_3, T_4]^T$ is the system control vector. $f(x(t), u(t))$ represents the mapping relation among $\dot{x}$, x and u. C_d is the output matrix equaling to a diagonal identity matrix, and y is the system output.

III. Control Strategy Illustration

3.1. Control Framework

The proposed control framework consists of upper-level control, tire slip estimator, and lower-level control, as shown in Fig. 2. At each sample instant, the vehicle dynamic system and an embedded driver model constructed in the software CarSim, provide the longitudinal vehicle velocity, road adhesion factor, vehicle sideslip angle, yaw rate, and front wheels' steering angle to upper-level control. In upper-level control, regarding sideslip angle and yaw rate, the references are produced by steering angle, tire adhesion factor, and vehicle velocity, and the errors between target and feedback are calculated. Based on the errors, a LQR controller contributes to generate the external yaw moment for guaranteeing vehicle drive property and lateral stability. Meanwhile, the torques and speeds regarding IWMs are fed back into the tire slip estimator so that the longitudinal velocity of tire center, tire slip rate, and longitudinal slip stiffness can be observed. In lower-level control, based on estimated tire information, expected total traction torque and external yaw moment, MPCA controller is developed to allocate the torque command of IWMs for minimum of tire slip power loss and vehicle stability. Since the addressed CA is highly nonlinear and multiple-constraints coupled, the C/GMRES algorithm is delegated to solve the MPCA problem in a computationally efficient way. Here the equality constraints are merged into the optimization problem to reduce the solving complexity, and external penalty method is adopted in handling inequality constraints to meet the C/GMRES algorithm's application. As such, an unconstrained MPCA problem can be formulated, thus C/GMRES algorithm is applicable. Additionally, to extend the algorithm application, a KKT conditions based two-steps method is designed for initial solution solving. Finally, the torque command of IWMs is gained and inputs into the high-fidelity vehicle model of software Carsim.

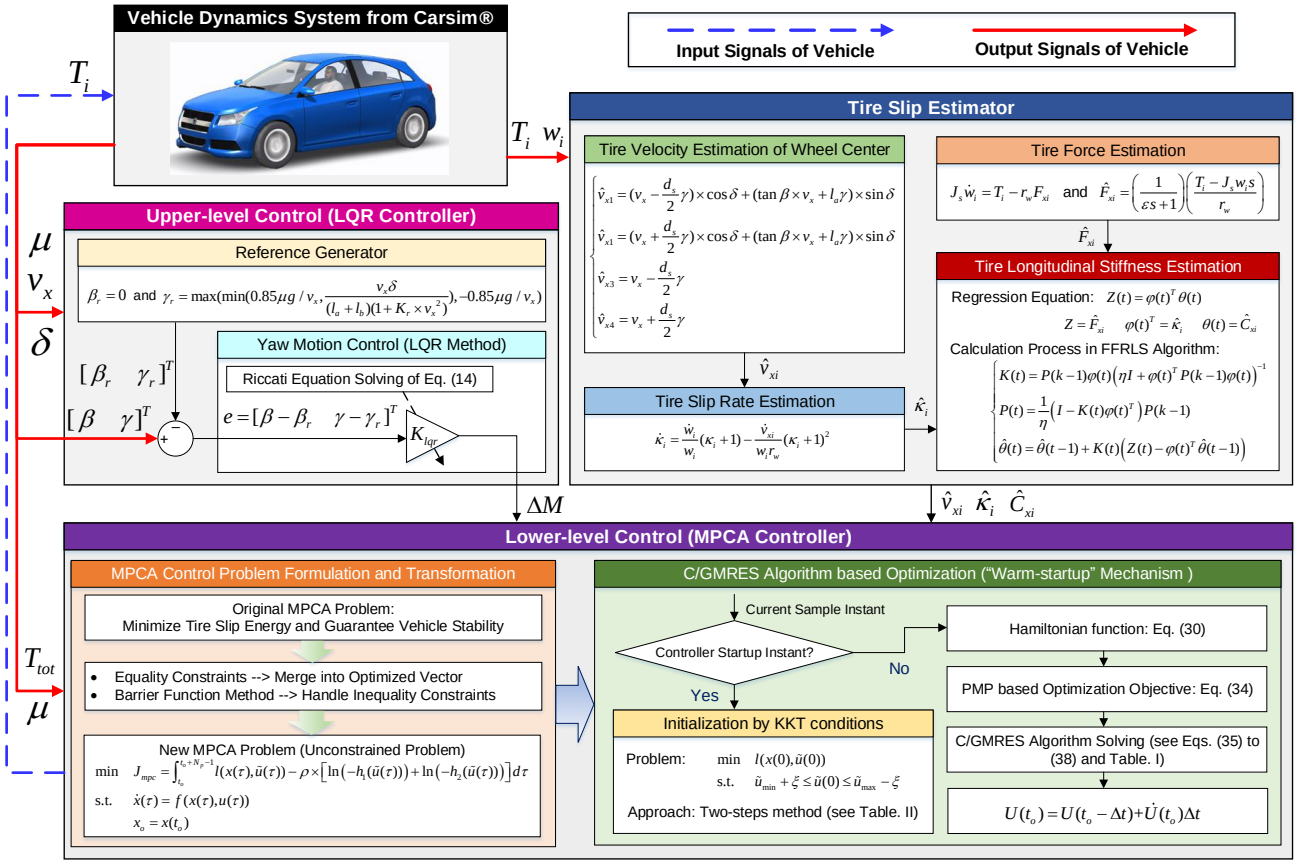

Fig. 2. Control framework schematic.

3.2. Upper-level Yaw Motion Control

The LQR controller is adopted in yaw motion control to meet the yaw motion stability. According to two DOF vehicle model of Eq. (1), the steady-state sideslip angle β_r and yaw rate γ_r can be expressed in the form of state update as,

$$\dot{x}_r = A_t x_r + D_t w_t \tag{11}$$

where $x_r = [\beta_r \quad \gamma_r]^T$. Here β_r is set as zero, and γ_r is determined by the following expression (Zhang and Göhlich, 2017).

$$\begin{cases} \gamma_r = \max(\min(0.85\mu g / v_x, \dfrac{v_x \delta}{(l_a + l_b)(1 + K_r \times v_x^2)}), -0.85\mu g / v_x) \\ K_r = m \times (l_a / C_r - l_b / C_f) / (l_a + l_b)^2 \end{cases} \tag{12}$$

where K_r denotes the understeer gradient, and g is the gravitational acceleration. From Eqs. (1) and (11), the error system of yaw motion control can be formulated as (Wang et al., 2019),

$$\dot{e} = A_t e + B_t u_t \tag{13}$$

where $e = [\beta - \beta_r \quad \gamma - \gamma_r]^T$ is the error variable. Then the performance index of LQR controller is defined as,

$$J_{lqr} = \|e\|^2_{Q_{lqr}} + \|u_t\|^2_{R_{lqr}} \tag{14}$$

where $\|\cdot\|$ represents the Euclidean norm. Q_{lqr} and R_{lqr} are the diagonal weight matrixes related to e and u_t, respectively. By solving the Riccati equation of Eq. (14) (Nguyen et al., 2019), the control gain vector of LQR K_{lqr} can be gained, and the expected external yaw moment can be calculated by $\Delta M = K_{lqr} e$. To gain the sideslip angle β, the longitudinal velocity v_x, and road adhesion factor μ, extensive studies of advanced estimators (Qin et al., 2018, Guo et al., 2018) have been carried out with high accuracy. Moreover, the IMU is easily adopted in practice to measure the yaw rate γ (Lenzo et al., 2020). Thus these variables are assumed to be obtainable in this paper.

3.3. Tire Slip Estimator

From Section 2.2, the tire slip rate model is not applicable unless v_{xi}, T_i, C_{xi} and w_i are known. Owing to the independently driven capacity of DDEVs, T_i and w_i can be gained by IWMs' feedback. The state update expressions of estimated velocity $\hat{v}_{xi}$ are furnished as,

$$\begin{cases} \hat{v}_{x1} = (v_x - \frac{d_s}{2}\gamma) \times \cos\delta + (\tan\beta \times v_x + l_a\gamma) \times \sin\delta \\ \hat{v}_{x1} = (v_x + \frac{d_s}{2}\gamma) \times \cos\delta + (\tan\beta \times v_x + l_a\gamma) \times \sin\delta \\ \hat{v}_{x3} = v_x - \frac{d_s}{2}\gamma \\ \hat{v}_{x4} = v_x + \frac{d_s}{2}\gamma \end{cases} \tag{15}$$

where d_s is the wheel track width. Based on the derivative of v_{xi} and w_i regarding time, $\hat{\kappa}_i$ can be calculated by Eq. (8). From Eq. (5), the estimated wheel force $\hat{F}_{xi}$ can be expressed (Maeda et al., 2012):

$$\hat{F}_{xi} = \left(\frac{1}{\varepsilon s + 1}\right)\left(\frac{T_i - J_s w_i s}{r_w}\right) \tag{16}$$

where s is the Laplace operator. The first order inertial link $\frac{1}{\varepsilon s+1}$ is applied to eliminate noise caused by taking differential of wheel rotation speed w_i. Based on $F_{xi}=C_{xi}\kappa_i$, the estimated tire longitudinal stiffness $\hat{C}_{xi}$ can be calculated by FFRLS algorithm. The regression equation in FFRLS algorithm is defined:

$$Z(t)=\varphi(t)^T\theta(t) \tag{17}$$

The calculation process of FFRLS algorithm is given as,

$$\begin{cases} K(t)=P(k-1)\varphi(t)\left(\eta I+\varphi(t)^T P(k-1)\varphi(t)\right)^{-1} \\ P(t)=\frac{1}{\eta}\left(I-K(t)\varphi(t)^T\right)P(k-1) \\ \hat{\theta}(t)=\hat{\theta}(t-1)+K(t)\left(Z(t)-\varphi(t)^T\hat{\theta}(t-1)\right) \end{cases} \tag{18}$$

where $Z=\hat{F}_{xi}$ is the measured output, $\varphi(t)^T=\hat{\kappa}_i$ is the input regression, and $\theta(t)=\hat{C}_{xi}$ is the pseudo-parameter. K is the recursive gain matrix, P is the covariance matrix, and η is the forgetting factor which is arranged within 0 to 1. If the regression $\hat{\kappa}_i$ equals zero, the persistent excitation is not satisfied. Thus, to avoid the saltation of $\hat{C}_{xi}$ caused by extensively small $\hat{\kappa}_i$, Eq. (18) is not updated if $\left|\hat{\kappa}_i\right|\le\kappa_{i\_thres}$. Fig. 3 to 5 show the estimation results under single lane change (SLC) cycle with target vehicle velocity of 80 km/h and road adhesion factor of 0.85. As yielded in Fig. 3, adopting Eqs. (8) and (15) can achieve the accurate estimation of κ_i. The result of $\hat{C}_{xi}$ is shown in Fig. 4. By taking the update mechanism in FFRLS, the great saltation of $\hat{C}_{xi}$ is eliminated in accord with physical characteristics of tires. To verify the precision of $\hat{C}_{xi}$, the comparison between real tires' longitudinal forces and the values of reverse calculation by FFRLS algorithm is shown in Fig. 5, namely F_{xi} and $\varphi(t)^T\theta(t)$. The difference between two variables is relatively small, which means the adopted FFRLS algorithm is accurate enough for controller application.

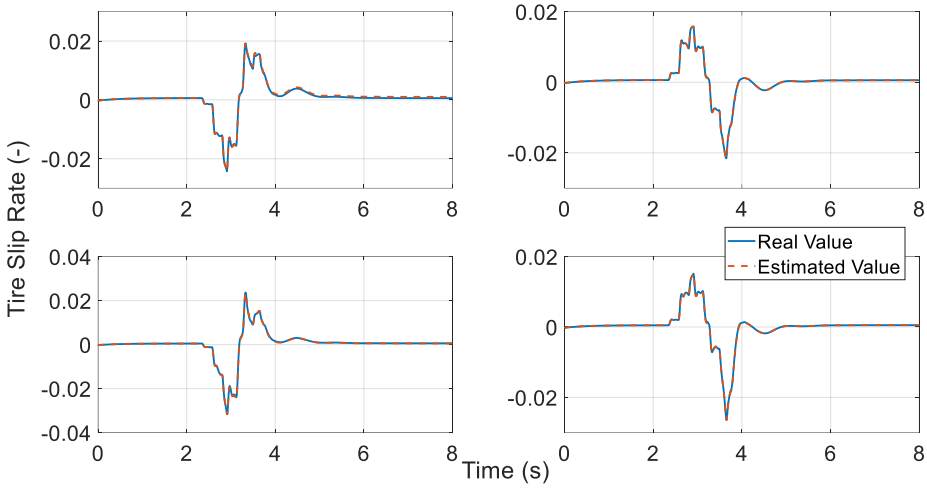

Fig. 3. Tire slip rate estimation result.

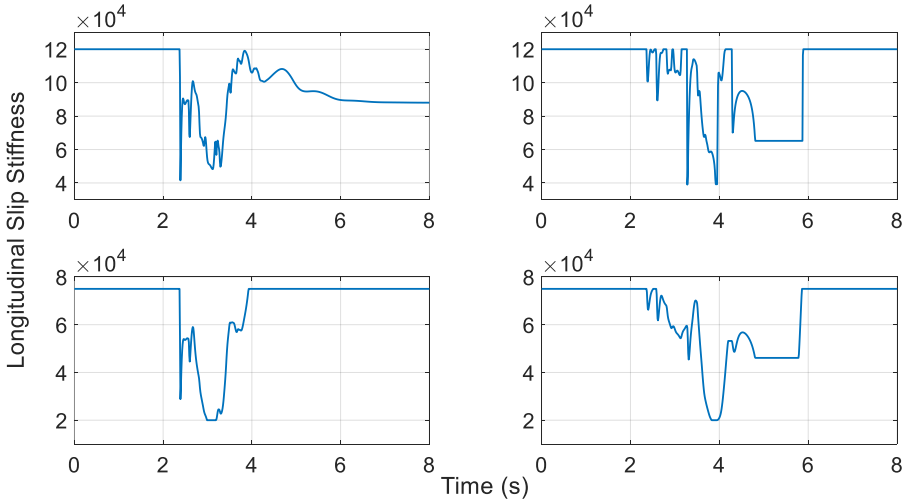

Fig. 4. Estimation of tire longitudinal slip stiffness.

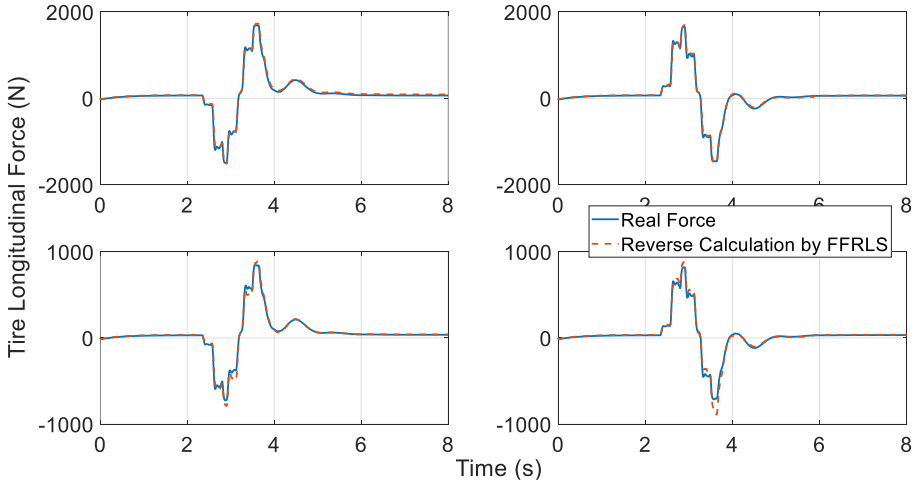

Fig. 5. Tire longitudinal force comparison between real value and value of reverse calculation by FFRLS algorithm.

3.4. Lower-level Torque Allocation Control

The main objective in lower-level control is to allocate the torques among IWMs for tire slip power loss minimization and vehicle stability. In the following, the MPC control problem is constructed first, and then a modified C/GMRES algorithm is introduced.

3.4.1. Control Allocation Problem Construction

The control problem P_0 for the addressed issue can be furnished as,

$$\begin{aligned} \min \quad & J_{mpc} = \int_{t_o}^{t_o+N_p-1} l(x(\tau),u(\tau))d\tau \\ \text{s.t.} \quad & \dot{x}(\tau) = f(x(\tau),u(\tau)) \\ & x_o = x(t_o) \\ & c(x(t_o),u(\tau)) = 0 \\ & h(x(t_o),u(\tau)) \le 0 \end{aligned} \tag{19}$$

where $c(x(t_o),u(\tau))$ and $h(x(t_o),u(t))$ represent the equality and inequality constraints in MPCA, respectively. x_o is the initial state of MPCA, and N_p represents the predictive horizon. The performance cost $l(x(\tau),u(\tau))$ is presented as,

$$l(x(\tau),u(\tau)) = l_1(x(\tau),u(\tau)) + l_2(x(\tau),u(\tau)) \tag{20}$$

$$\begin{cases} l_1(x(\tau),u(\tau)) = P_{loss}(\tau)^T Q P_{loss}(\tau) = \sum_{i=1}^{4} q_i \left(v_{xi}(\tau)\kappa_i(\tau)\right)^2 \left(\frac{T_i(\tau) - J_s \dot{w}_i(\tau)}{r_w}\right)^2 \\ l_2(x(\tau),u(\tau)) = \left(u(\tau) - u(t_o - \Delta t)\right)^T R \left(u(\tau) - u(t_o - \Delta t)\right) = \sum_{i=1}^{4} r_i \left(T_i(\tau) - T_i(t_o - \Delta t)\right)^2 \end{cases} \tag{21}$$

where $P_{loss} = [F_{x1}\kappa_1 v_{x1} \quad F_{x2}\kappa_2 v_{x2} \quad F_{x3}\kappa_3 v_{x3} \quad F_{x4}\kappa_4 v_{x4}]^T$ denotes the longitudinal slip power loss vector of tires (Kobayashi et al., 2018). $Q = \mathrm{diag}\left(q_1 \quad q_2 \quad q_3 \quad q_4\right)$ and $R = \mathrm{diag}\left(r_1 \quad r_2 \quad r_3 \quad r_4\right)$ are the diagonal weight matrixes. The cost $l_1(x(\tau),u(\tau))$ and $l_2(x(\tau),u(\tau))$ are adopted to minimize the square norm of tires' slip power loss and the square norm of IWM's torque vibration, respectively.

To satisfy the longitudinal and yaw drive property, the equality constraint of virtual controls is set as,

$$c(x(t_o),u(\tau)) = \chi u(\tau) - \upsilon \tag{22}$$

where $\chi = \begin{bmatrix} 1 & 1 & 1 & 1 \\ -\frac{d_s}{2r_w} & \frac{d_s}{2r_w} & -\frac{d_s}{2r_w} & \frac{d_s}{2r_w} \end{bmatrix}$ is the coefficient matrix, and $\upsilon = [T_{tot} \quad \Delta M]^T$ is the virtual control vector. T_{tot} denotes the expected total traction torque from driver.

The inequality constraints are provided by,

$$h(x(t_o), u(\tau)) = [(u - u_{\max})^T \quad (u_{\min} - u)^T]^T \le 0 \tag{23}$$

where $u_{\max} = [u_{\max 1} \quad u_{\max 2} \quad u_{\max 3} \quad u_{\max 4}]^T$, and $u_{\max i}$ represents the maximum torque output of the i th IWM. $u_{\min} = [u_{\min 1} \quad u_{\min 2} \quad u_{\min 3} \quad u_{\min 4}]^T$, and $u_{\min i}$ represents the minimum torque output of the i th IWM. Based on the tire adhesion circle theory (Zhang and Göhlich, 2017), the tire forces should meet the relationship $\frac{F_{xi}{}^2 + F_{yi}{}^2}{\mu^2 F_{zi}{}^2} \le 1$ to ensure vehicle stability. Thus the following inequality limits are imposed:

$$\begin{cases} u_{\max i} = \min(T_{\max i}, r_w \times \sqrt{\eta \times \mu^2 F_{zi}{}^2 - F_{yi}{}^2}) \\ u_{\min i} = \max(T_{\min i}, -r_w \times \sqrt{\eta \times \mu^2 F_{zi}{}^2 - F_{yi}{}^2}) \end{cases} \tag{24}$$

where $T_{\max i}$ and $T_{\min i}$ are the maximum and minimum torque physical limits of the i th IWM, respectively. η is the margin coefficient. Since the model errors between controller and real vehicle are inevitable, η is set as 0.85 to meet $\frac{F_{xi}{}^2 + F_{yi}{}^2}{\mu^2 F_{zi}{}^2} \le 1$.

Remark 1: It is noteworthy that $l_2(x(\tau), u(\tau))$ is of significance in control effects of MPCA. Given that the dynamic response of IWM can be seen as first-order inertia link, it is quite difficult for an IWM to make its real torque output to approximate the control command if the control command is jittered. In addition, the unnecessary vibration of command will entail undesirable tire slip and indirectly influence the IWMs' lifetime to some extent.

Remark 2: From the expression of l_1 in Eq. (21), the cost item $q_i\left(v_{xi}(\tau)\kappa_i(\tau)\right)^2 (\frac{T_i(\tau) - J_s \dot{w}_i(\tau)}{r_w})^2$ can be approximately seen as $q_i\left(v_{xi}(\tau)\kappa_i(\tau)\right)^2 T_i(\tau)^2$ since $\dot{w}_i(\tau)$ is relatively smaller under most of cases. Given that greater slip rate generally occurs under higher vehicle velocity, the time-varying weight item $q_i\left(v_{xi}(\tau)\kappa_i(\tau)\right)^2$ is

effective to penalize the enlargement of $T_i(\tau)$ for reducing $\kappa_i(\tau)$. In other words, by minimizing l_1, the slip rate of each tire can be adaptively restricted, and this is why the constraints of slip rate are not imposed in the proposed MPCA. Numerical simulations in Section IV also validate this viewpoint.

3.4.2. Application of Modified C/GMRES Algorithm

The C/GMRES algorithm is applied to efficiently solve the addressed MPCA problem. To reduce the control complexity, a new optimized vector is redefined to reduce the number of optimized variables by merging equality constraints into optimization. Since the original C/GMRES algorithm cannot handle the inequality constraints, the barrier function method is adopted to construct an equivalent optimization problem satisfying system boundaries. Finally, the MPCA problem P_0 is transformed to an unconstrained one, and the solution existence and uniqueness are verified. To extend the algorithm application, a fast initialization approach based on KKT optimality conditions is also developed in MPCA.

1) Control Problem Transformation

Based on equality constraint (22), the following expression is hold (Li et al., 2015):

$$\begin{cases} T_3 = \dfrac{T_{tot}}{2} - \dfrac{r_w \Delta M}{d_s} - T_1 \\ T_4 = \dfrac{T_{tot}}{2} + \dfrac{r_w \Delta M}{d_s} - T_2 \end{cases} \tag{25}$$

By Eq. (25), a new optimized vector $\tilde{u} = [\tilde{u}_1 \quad \tilde{u}_2]^T = [T_1 \quad T_2]^T$ can be defined, and

$$u = Z_1 \tilde{u} + Z_2 = \begin{bmatrix} 1 & 0 \\ 0 & 1 \\ -1 & 0 \\ 0 & -1 \end{bmatrix} \tilde{u} + \begin{bmatrix} 0 \\ 0 \\ \dfrac{T_{tot}}{2} - \dfrac{r_w \Delta M}{d_s} \\ \dfrac{T_{tot}}{2} + \dfrac{r_w \Delta M}{d_s} \end{bmatrix} \tag{26}$$

By Eq. (26), the equality constraints (22) can be merged into state updates, and the number of optimized variables in proposed MPCA can be reduced by $3 \times N_p$ (i.e., Lagrange multiplier, T_3, and T_4 at each predictive instant for C/GMRES algorithm), which considerably migrates the calculation burden. To satisfy the limits of T_3 and T_4, a new limits of $\tilde{u}$ should be imposed:

$$\begin{cases} \tilde{u}_{\max 1} = \min\left(u_{\max 1}, \dfrac{T_{tot}}{2} - \dfrac{r_w \Delta M}{d_s} - u_{\min 3} \right), \tilde{u}_{\min 1} = \max\left(u_{\min 1}, \dfrac{T_{tot}}{2} - \dfrac{r_w \Delta M}{d_s} - u_{\max 3} \right) \\ \tilde{u}_{\max 2} = \min\left(u_{\max 2}, \dfrac{T_{tot}}{2} + \dfrac{r_w \Delta M}{d_s} - u_{\min 4} \right), \tilde{u}_{\min 2} = \max\left(u_{\min 2}, \dfrac{T_{tot}}{2} + \dfrac{r_w \Delta M}{d_s} - u_{\max 4} \right) \end{cases} \tag{27}$$

The inequality constraint $h(x(t_o), \tilde{u}(\tau)) = [h_1 \quad h_2]^T$ related to $\tilde{u}$ can be set up as,

$$\begin{cases} h_1 = (\tilde{u}_1 - \dfrac{\tilde{u}_{\max 1} + \tilde{u}_{\min 1}}{2})^2 - (\dfrac{\tilde{u}_{\max 1} - \tilde{u}_{\min 1}}{2})^2 \le 0 \\ h_2 = (\tilde{u}_2 - \dfrac{\tilde{u}_{\max 2} + \tilde{u}_{\min 2}}{2})^2 - (\dfrac{\tilde{u}_{\max 2} - \tilde{u}_{\min 2}}{2})^2 \le 0 \end{cases} \tag{28}$$

To handle Eq. (28) in C/GMRES algorithm, the barrier function method (Boyd et al., 2006) is adopted, and the original control problem P_0 can be rewritten to be a new one P_1:

$$\begin{aligned} \min \quad & J_{mpc} = \int_{t_o}^{t_o + N_p - 1} l(x(\tau), \tilde{u}(\tau)) - \rho \times \left[\ln\left(-h_1(\tilde{u}(\tau))\right) + \ln\left(-h_2(\tilde{u}(\tau))\right) \right] d\tau \\ \text{s.t.} \quad & \dot{x}(\tau) = f(x(\tau), u(\tau)) \\ & x_o = x(t_o) \end{aligned} \tag{29}$$

where ρ is the weight coefficient of barrier function. $-\rho \times \left[\ln\left(-h_1(\tilde{u}(\tau))\right) + \ln\left(-h_2(\tilde{u}(\tau))\right) \right]$ is the equivalent cost by log barrier functions, which is able to avoid exceeding the inequality constraints of Eq. (28). Specifically, it is verified (Nocedal and Wright, 2006) that by the log barrier functions, the optimal solution of unconstrained problem (like P_1) infinitely closes to that of original problem (like P_0) when $\rho \to 0$.

2) C/GMRES Algorithm and Analysis

Based on Eq. (29), the Hamiltonian function of problem P_1 can be expressed as,

$$H(x, \tilde{u}) = l(x, \tilde{u}) - \rho \times \left[\ln\left(-h_1(\tilde{u}(\tau))\right) + \ln\left(-h_2(\tilde{u}(\tau))\right) \right] + \lambda^T f(x, \tilde{u}) \tag{30}$$

where $\lambda = [\lambda_1 \quad \lambda_2 \quad \lambda_3 \quad \lambda_4]^T$ is the co-state vector. The differentials of Eq. (30) with respect to x can be yielded as,

$$
\begin{cases}
\dfrac{\partial H}{\partial \kappa_1} = 2q_1(T_1 - J_s\dot{w}_1)^2(\dfrac{v_{x1}}{r_w})^2\kappa_1 + \lambda_1\left(\dfrac{-r_wC_{x1}}{J_sw_1} + \dfrac{T_1 - 2r_wC_{x1}\kappa_1}{J_sw_1} - 2\dfrac{a_{x1}}{w_1r_w}(\kappa_1+1)\right) \\
\dfrac{\partial H}{\partial \kappa_2} = 2q_2(T_2 - J_s\dot{w}_2)^2(\dfrac{v_{x2}}{r_w})^2\kappa_2 + \lambda_2\left(\dfrac{-r_wC_{x2}}{J_sw_2} + \dfrac{T_2 - 2r_wC_{x2}\kappa_2}{J_sw_2} - 2\dfrac{a_{x2}}{w_2r_w}(\kappa_2+1)\right) \\
\dfrac{\partial H}{\partial \kappa_3} = 2q_3(\dfrac{T_{tot}}{2} - \dfrac{r_w\Delta M}{d_s} - T_1 - J_s\dot{w}_3)^2(\dfrac{v_{x3}}{r_w})^2\kappa_3 + \lambda_3\left(\dfrac{-r_wC_{x3}}{J_sw_3} + \dfrac{\dfrac{T_{tot}}{2} - \dfrac{r_w\Delta M}{d_s} - T_1 - 2r_wC_{x3}\kappa_3}{Jw_3} - 2\dfrac{a_{x3}}{w_3r_w}(\kappa_3+1)\right) \\
\dfrac{\partial H}{\partial \kappa_3} = 2q_3(\dfrac{T_{tot}}{2} + \dfrac{r_w\Delta M}{d_s} - T_1 - J_s\dot{w}_3)^2(\dfrac{v_{x3}}{r_w})^2\kappa_3 + \lambda_3\left(\dfrac{-r_wC_{x3}}{J_sw_3} + \dfrac{\dfrac{T_{tot}}{2} + \dfrac{r_w\Delta M}{d_s} - T_1 - 2r_wC_{x3}\kappa_3}{Jw_3} - 2\dfrac{a_{x3}}{w_3r_w}(\kappa_3+1)\right)
\end{cases}
\tag{31}
$$

Since there is no terminal cost in problem P_1 and x_o is given, the updates with respect to states and co-states can be yielded as below, respectively,

$$
\begin{cases}
\kappa_1(\tau+1) = \kappa_1(\tau) + \left(\dfrac{T_1(\tau) - r_wC_{x1}\kappa_1(\tau)}{J_sw_1}(\kappa_1(\tau)+1) - \dfrac{a_{x1}}{w_1r_w}(\kappa_1(\tau)+1)^2\right)\Delta\tau \\
\kappa_2(\tau+1) = \kappa_2(\tau) + \left(\dfrac{T_2(\tau) - r_wC_{x2}\kappa_2(\tau)}{J_sw_2}(\kappa_2(\tau)+1) - \dfrac{a_{x2}}{w_2r_w}(\kappa_2(\tau)+1)^2\right)\Delta\tau \\
\kappa_3(\tau+1) = \kappa_3(\tau) + \left(\dfrac{\dfrac{T_{tot}}{2} - \dfrac{r_w\Delta M}{d_s} - T_1(\tau) - r_wC_{x3}\kappa_3(\tau)}{J_sw_3}(\kappa_3(\tau)+1) - \dfrac{a_{x3}}{w_3r_w}(\kappa_3(\tau)+1)^2\right)\Delta\tau \\
\kappa_4(\tau+1) = \kappa_4(\tau) + \left(\dfrac{\dfrac{T_{tot}}{2} - \dfrac{r_w\Delta M}{d_s} - T_2(\tau) - r_wC_{x4}\kappa_4(\tau)}{J_sw_4}(\kappa_4(\tau)+1) - \dfrac{a_{x4}}{w_4r_w}(\kappa_4(\tau)+1)^2\right)\Delta\tau
\end{cases}
\tag{32}
$$

$$
\begin{cases}
\lambda_1(\tau) = \lambda_1(\tau+1) + \left(\dfrac{\partial H}{\partial \kappa_1}(x(\tau+1), \tilde{u}(\tau+1))\right)\Delta\tau \\
\lambda_2(\tau) = \lambda_2(\tau+1) + \left(\dfrac{\partial H}{\partial \kappa_2}(x(\tau+1), \tilde{u}(\tau+1))\right)\Delta\tau \\
\lambda_3(\tau) = \lambda_3(\tau+1) + \left(\dfrac{\partial H}{\partial \kappa_3}(x(\tau+1), \tilde{u}(\tau+1))\right)\Delta\tau \\
\lambda_4(\tau) = \lambda_4(\tau+1) + \left(\dfrac{\partial H}{\partial \kappa_4}(x(\tau+1), \tilde{u}(\tau+1))\right)\Delta\tau
\end{cases}
\tag{33}
$$

Based on the optimality conditions of PMP (Kirk, 2004-04-30), the MPCA problem is transformed to be an optimal control one:

$$F(U(t_o),x_o(t))=\begin{bmatrix} \frac{\partial H}{\partial T_1}(x(t_o),\tilde{u}(t_o),\lambda^T(t_o)) \\ \frac{\partial H}{\partial T_2}(x(t_o),\tilde{u}(t_o),\lambda^T(t_o)) \\ \vdots \\ \frac{\partial H}{\partial T_1}(x(t_o+N_p-1),\tilde{u}(t_o+N_p-1),\lambda^T(t_o+N_p-1)) \\ \frac{\partial H}{\partial T_2}(x(t_o+N_p-1),\tilde{u}(t_o+N_p-1),\lambda^T(t_o+N_p-1)) \end{bmatrix}=0 \tag{34}$$

where the optimized vector is,

$$U=[T_1(t_o)\quad T_2(t_o)\quad \cdots\quad T_1(\tau)\quad T_2(\tau)\quad \cdots\quad T_1(t_o+N_p-1)\quad T_2(t_o+N_p-1)]^T \tag{35}$$

and,

$$\begin{cases} \frac{\partial H}{\partial T_1}=2q_1(\frac{v_{x1}\kappa_1(\tau)}{r_w})^2(T_1(\tau)-J_s\dot{w}_1)-2q_3(\frac{v_{x3}\kappa_3(\tau)}{r_w})^2(\frac{T_{tot}}{2}-\frac{r_w\Delta M}{d_s}-T_1(\tau)-J_s\dot{w}_3)+ \\ \quad 2r_1(T_1(\tau)-T_1(t_o-\Delta t))-2r_3(\frac{T_{tot}}{2}-\frac{r_w\Delta M}{d_s}-T_1(\tau)-T_3(t_o-\Delta t))-2\rho\frac{1}{h_1(\tau)}(T_1(\tau)-\frac{\tilde{u}_{\max 1}+\tilde{u}_{\min 1}}{2}) \\ \quad +\left(\lambda_1(\tau)\frac{1}{J_s w_1}(\kappa_1(\tau)+1)-\lambda_3(\tau)\frac{1}{J_s w_3}(\kappa_3(\tau)+1)\right) \\ \frac{\partial H}{\partial T_2}=2q_2(\frac{v_{x2}\kappa_2(\tau)}{r_w})^2(T_2(\tau)-J_s\dot{w}_2)-2q_3(\frac{v_{x4}\kappa_4(\tau)}{r_w})^2(\frac{T_{tot}}{2}+\frac{r_w\Delta M}{d_s}-T_2(\tau)-J_s\dot{w}_4)+ \\ \quad 2r_2(T_2(\tau)-T_2(t_o-\Delta t))-2r_4(\frac{T_{tot}}{2}+\frac{r_w\Delta M}{d_s}-T_2(\tau)-T_4(t_o-\Delta t))-2\rho\frac{1}{h_2(\tau)}(T_2(\tau)-\frac{\tilde{u}_{\max 2}+\tilde{u}_{\min 2}}{2}) \\ \quad +\left(\lambda_2(\tau)\frac{1}{J_s w_2}(\kappa_2(\tau)+1)-\lambda_4(\tau)\frac{1}{J_s w_4}(\kappa_4(\tau)+1)\right) \end{cases} \tag{36}$$

Ideally, solving Eq. (34) is realizable by iterative optimization algorithms, like sequence quadratic programming (SQP) methods and interior-point method etc., but causing expensive calculation burden. To avoid the calculations of Jacobian matrix, Hessian matrix and inverse in Eq. (34), the continuation method is applied (Allgower and Georg, 2003), and Eq. (34) can be rewritten as a linear dynamic system:

$$\dot{F}(U_o(t),x_o(t),t)=-\psi_s F(U(t_o),x_o(t),t) \tag{37}$$

where ψ_s is the stability matrix, aiming to stabilize $F(U(t_o), x_o(t), t)$ at original. If $\frac{\partial F}{\partial U}(U(t_o), x(t_o), t)$ is nonsingular, the solution $\dot{U}(t_o)$ can be determined by,

$$\dot{U}(t_o) = [\frac{\partial F}{\partial U}(U(t_o), x_o(t), t)]^{-1}[-\psi_s F(U(t_o), x_o(t), t) - \frac{\partial F}{\partial x}(U(t_o), x_o(t), t) \times \dot{x}(t)] \tag{38}$$

To further avoid the computational labor caused by inverse operation of $[\frac{\partial F}{\partial U}(U_o(t), x_o(t), t)]^{-1}$, the forward difference approximation is imposed, and then the GMRES algorithm can be adopted to search the optimal solution $\dot{U}$ (Kelley, 1995). The state update step $\Delta\tau$ is set equaling to control sample step Δt for simplification. At each sample, $U(t)$ is determined by summing up $U(t_o)$ and $\dot{U} \cdot \Delta t$, and the first group of control command (i.e., $\tilde{u}$) in $U(t)$ is adopted to calculate four IWMs' torque commands by Eq. (26). For more details, the calculation steps of C/GMRES algorithm are summarized in Table I.

Table I. C/GMRES algorithm illustration.

C/GMRES algorithm
1. Initialize $t = 0$ and $x_o = x(0)$. Calculate $U(0)$ numerically by function $F(U(0), x_o(0), 0) = 0$;
2. The first control variable of $U(0)$ outputs in MPCA;
3. At next sample cycle $s \in [t \quad t + \Delta t]$, obtain the feedback states of system and set $x_o = x(t_o)$. The difference of states at the last moment and current moment is calculated by $\Delta x(t_o) = x(t_o) - x(t_o - 1)$;
4. Given U_{k-1}, $x(t_o)$, $\Delta x(t_o) / \Delta t$, size of difference grids ζ, and allowed maximum iteration number $k_{\max}$, the optimal $\dot{U}_k$ is gained by GMRES method with forward difference approximation;
5. Set $U_k = U_{k-1} + \dot{U}_k \Delta t$
6. Update $t = t + \Delta t$ and $k = k + 1$;
7. Return to step 2.

It is noteworthy that the optimal solution of C/GMRES algorithm is existent and exclusive only if $\frac{\partial F}{\partial U}$ is invertible (Ohtsuka, 2004). Moreover, one can find that from Eq. (34), $\frac{\partial F}{\partial U}$ is in fact a $N_p \times N_p$ block diagonal matrix, whose each block is a Hessian matrix of Hamiltonian function, namely $\frac{\partial^2 H}{\partial u^2}$. Thus, whether $\frac{\partial F}{\partial U}$ is invertible, can be judged by analyzing the singularity of $\frac{\partial^2 H}{\partial u^2}$. By Eq. (36), the expression of $\frac{\partial^2 H}{\partial u^2}$ is furnished as,

$$\frac{\partial^2 H}{\partial u^2}=\begin{bmatrix} \frac{\partial^2 H}{\partial T_1^2} & \frac{\partial^2 H}{\partial T_1 \partial T_2} \\ \frac{\partial^2 H}{\partial T_2 \partial T_1} & \frac{\partial^2 H}{\partial T_2^2} \end{bmatrix}$$

$$=\begin{bmatrix} 2q_1(\frac{v_{x1}\kappa_1}{r_w})^2+2q_3(\frac{v_{x3}\kappa_3}{r_w})^2+2r_1 & 0 \\ +2r_3-2\rho\left(\frac{h_1-2(T_1-\frac{\tilde{u}_{\max 1}+\tilde{u}_{\min 1}}{2})^2}{h_1^2}\right) & \\ 0 & 2q_2(\frac{v_{x2}\kappa_2}{r_w})^2+2q_4(\frac{v_{x4}\kappa_4}{r_w})^2+2r_2 \\ & +2r_4-2\rho\left(\frac{h_2-2(T_2-\frac{\tilde{u}_{\max 2}+\tilde{u}_{\min 2}}{2})^2}{h_2^2}\right) \end{bmatrix} \tag{39}$$

The discussion regarding singularity of $\frac{\partial^2 H}{\partial u^2}$ is illustrated as below.

Proposition 1: When the feasible region exists and C/GMRES algorithm in MPCA is proceeding after initialization, the inequality constraint $h(\cdot)$ is always hold by $U(t_o-\Delta t)$ that satisfies $h(\cdot)$.

Proof: The optimization of C/GMRES algorithm is essential to minimize the value difference between each side of equality sign in Eq. (34) according to optimality conditions of PMP. The contradiction method is adopted here for proof. Since $U(t_o-\Delta t)$ satisfies the inequality $h(\cdot)$ and the feasible region of optimization exists, $\frac{\partial H}{\partial T_1}\to\infty\neq 0$ and/or $\frac{\partial H}{\partial T_2}\to\infty\neq 0$ by Eq. (36) if $\dot{U}(t_o)$ by C/GMRES algorithm makes $h(\cdot)\to 0$. As such, by Eq. (34), the value difference by GMRES algorithm leads to $\infty=0$, which is obviously incorrect and inconsistent to the PMP conditions. Thus to minimize the optimization cost, C/GMRES algorithm should choose the descending search direction of minimizing residual between each side of equality sign in Eq. (34) ; that is, under the case in proposition 1, the barrier function (29) is applicable to guarantee the inequality constraints. For calculation accuracy of C/GMRES algorithm, a detailed error analysis is provided in (Ohtsuka, 2004).

Proposition 2: When C/GMRES algorithm in MPCA is proceeding after initialization, $\frac{\partial^2 H}{\partial u^2}$ is positive definite and invertible if $U(t_o - \Delta t)$ satisfies the inequality constraint.

Proof: From proposition 1 and the assumption that the inequality constraint $h(\cdot)$ by $U(t_o - \Delta t)$ is hold, $-2\rho\left(\frac{h_1 - 2(T_1 - \frac{\tilde{u}_{\max 1} + \tilde{u}_{\min 1}}{2})^2}{h_1^{\,2}}\right) > 0$ and $-2\rho\left(\frac{h_2 - 2(T_2 - \frac{u_{\max 2} + u_{\min 2}}{2})^2}{h_2^{\,2}}\right) > 0$. Since the weight matrixes Q and R are always greater than zeros, there is,

$$\begin{cases} 2q_1(\frac{v_{x1}\kappa_1}{r_w})^2 + 2q_3(\frac{v_{x3}\kappa_3}{r_w})^2 + 2r_1 + 2r_3 - 2\rho\left(\frac{h_1 - 2(T_1 - \frac{\tilde{u}_{\max 1} + \tilde{u}_{\min 1}}{2})^2}{h_1^{\,2}}\right) > 0 \\ 2q_2(\frac{v_{x2}\kappa_2}{r_w})^2 + 2q_4(\frac{v_{x4}\kappa_4}{r_w})^2 + 2r_2 + 2r_4 - 2\rho\left(\frac{h_2 - 2(T_2 - \frac{\tilde{u}_{\max 2} + \tilde{u}_{\min 2}}{2})^2}{h_2^{\,2}}\right) > 0 \end{cases} \tag{40}$$

Therefore, $\frac{\partial^2 H}{\partial u^2}$ is positive definite and invertible. That is, $\frac{\partial F}{\partial U}$ is also positive definite and invertible since its diagonal blocks are comprised of $\frac{\partial^2 H}{\partial u^2}$.

From propositions 1 and 2, $U(t_o - \Delta t)$ should satisfy the inequality constraint $h(\cdot)$ so that $\frac{\partial F}{\partial U}$ is invertible. In other words, for addressed problem P_1, the inequality constraints and the optimization effects can be both guaranteed as long as $h(\cdot)$ by $U(0)$ is hold according to $U(t_o) = U(t_o - \Delta t) + \dot{U}(t_o)\Delta t$. The calculation of $U(0)$, namely the initialization in C/GMRES algorithm, is introduced in the following.

3) Initialization Calculation

For the addressed problem P_1, $U(0)$ can be set to be a zeros vector if the controller starts up when vehicle is standstill, and propositions 1 and 2 are hold. Moreover, from Table I, the numerical algorithms can also be adopted in gaining $U(0)$ in C/GMRES algorithm. That said, to enlarge the application of proposed method, this paper proposes a fast initialization approach for the addressed MPCA, which demands less computational labor but is

subject to propositions 1 and 2. Owing to the short sample step and predictive horizon in addressed MPCA, the initialization is approximately considered as a single-step MPCA optimization, namely $N_p = 1$ (Ohtsuka, 2004). Then $U(0)$ is calculated by $1_{N_p} \otimes \tilde{u}(0)$, where $1_{*\times *}$ means an identity matrix with the scale of $*\times *$, and $\otimes$ is the Kronecker product. It is noteworthy that by this manner the solution optimality is deteriorated to some extent, but it is acceptable since this method is only adopted in initialization and satisfy propositions 1 and 2. According to problem P_1, this single-step optimization is a QP issue, and a KKT condition (Guo et al., 2020a) based method can be employed for fast solving. The optimization problem can be expressed as,

$$\begin{aligned} &\min \quad l(x(0),\tilde{u}(0)) \\ &\text{s.t.} \quad \tilde{u}_{\min} + \xi \le \tilde{u}(0) \le \tilde{u}_{\max} - \xi \end{aligned} \tag{41}$$

where $\xi \in \Re^{2\times 1}$ is an extremely small offset vector with all the elements of 10^{-10} to guarantee the solution absolutely satisfying propositions 1 and 2. By Eq. (41), Lagrangian equation is presented as,

$$\begin{aligned} &L = l(x(0),\tilde{u}(0)) + \varepsilon_1^{\ T} \times (\tilde{u}_{\min} + \xi - \tilde{u}(0)) + \varepsilon_2^{\ T} \times (\tilde{u}(0) - \tilde{u}_{\max} + \xi) \\ &\text{s.t.} \begin{cases} \varepsilon_1^{\ T} \times (\tilde{u}_{\min} + \xi - \tilde{u}(0)) = 0 \\ \varepsilon_2^{\ T} \times (\tilde{u}(0) - \tilde{u}_{\max} + \xi) = 0 \\ \tilde{u}_{\min} + \xi - \tilde{u}(0) \le 0, \tilde{u}(0) - \tilde{u}_{\max} + \xi \le 0 \\ \varepsilon_1 \ge 0, \varepsilon_2 \ge 0 \end{cases} \end{aligned} \tag{42}$$

where ε_1 and ε_2 are the Lagrangian multiplier vectors regarding lower and higher limits, respectively. To solve Eq. (42), the two-steps method based on KKT conditions is proposed and summarized in Table II. Since the optimization in Eq. (41) is strictly convex, the globally optimal solution can be gained by the proposed two-steps initialization method, as detailed in (Zhang et al., 2017). Then, the initial solution $U(0)$ can be set as $1_{N_p \times 2} \otimes \tilde{u}^*(0)$.

Table II. KKT condition based method for initialization.

KKT condition based method
<u>1. Preliminary optimization:</u>
1) Optimization of Eq. (41) is considered as an unconstrained problem, and set $\varepsilon_1 = \varepsilon_2 = 0$. By $\frac{\partial L}{\partial \tilde{u}} = 0$, the solution $\tilde{u}^*(0)$ is gained.
2) If $\tilde{u}_{\min} + \xi \le \tilde{u}(0) \le \tilde{u}_{\max} - \xi$
Return $\tilde{u}^*(0)$ as the optimal solution
Else
go to secondary optimization
End
<u>2. Secondary optimization:</u>

1) For $i = 1, 2$

If the i th element in solution $\tilde{u}^*(0)$ is greater than the element in $\tilde{u}_{\max} - \xi$,

set the i th element of ε_1 equals to zero and the i th element in $\tilde{u}^*(0)$ equals to the i th element in $\tilde{u}_{\max} - \xi$.

If the i th element in solution $\tilde{u}^*(0)$ is less than the element in $\tilde{u}_{\min} + \xi$

set the i th element of ε_2 equals to zero and the i th element in $\tilde{u}^*(0)$ equals to the i th element in $\tilde{u}_{\min} + \xi$.

End

2) By $\dfrac{\partial L}{\partial \tilde{u}} = 0$, a new $\tilde{u}^*(0)$ is gained.

3) If $\tilde{u}_{\min} + \xi \le \tilde{u}(0) \le \tilde{u}_{\max} - \xi$

Return $\tilde{u}^*(0)$ as the optimal solution

Else

Repeat to secondary optimization

End

Now the introduction of proposed MPCA is completed. More specifically, an intuitive schematic is summarized in Fig. 6. At each sample instant, the tire information, vehicle velocity, and road adhesion factor are fed back and input into MPCA controller, and the target traction torque and external yaw moment are also given from upper-level control. For this MPCA, if the current sample instant is that of controller startup, the initialization calculation in Table II is conducted to gain the control command. Otherwise, at generic instant, the optimization operations in C/GMRES algorithm are implemented to find the command, shown in Table I. Afterwards, by optimized command and Eq. (26), four torque commands of IWMs are acquired and adopted for DDEV's control. It is noteworthy that for both initialization and generic period, the "warm-startup" mechanism is used and contributes to accelerate the solving convergence rate (Guo et al., 2020b), as depicted by purple lines in Fig. 6.

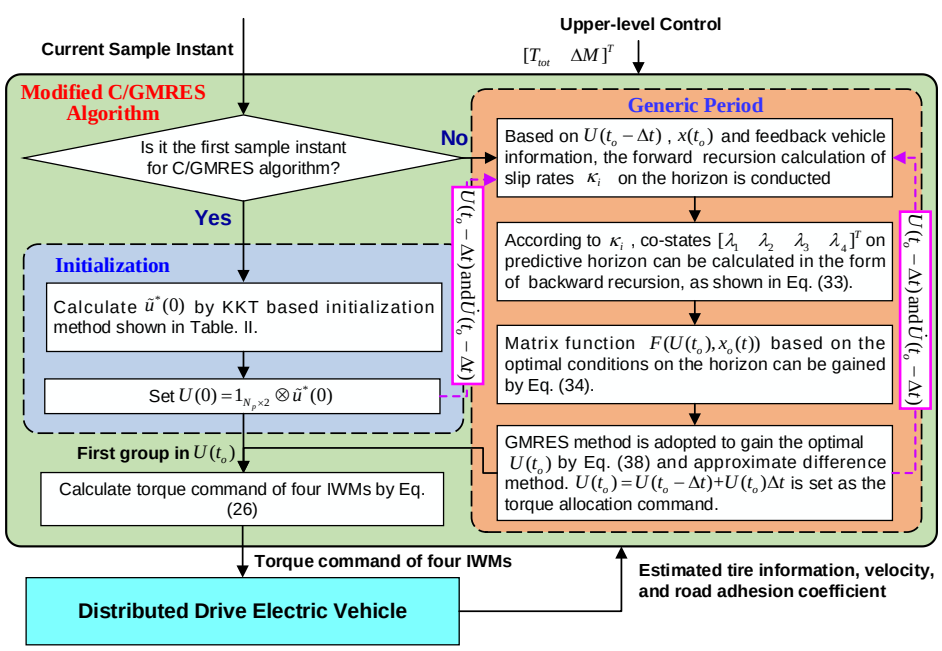

Fig. 6. Schematic of proposed C/GMRES algorithm based MPCA.

IV. Numerical Simulation and Analysis

The validations are carried out by co-simulation platform of Matlab and the high-fidelity software CarSim (Corporation, 2019) under Intel(R) Core(TM) i5-9400F CPU @ 2.9GHz desktop computer, where a CarSim-embedded driver model with 0.8 s preview time is adopted. Two cycles of SLC maneuver under high and low adhesion roads are employed as the test cycle, and the SLC profile is illustrated in Fig. 7. The parameters regarding vehicle and controller are listed in Table III. In this paper, the tire workload usage optimization (TWUO) allocation, and the MPCAs by SQP and active-set (AS) methods are conducted to verify the control effects and computational efficiency of proposed MPCA by comparisons, respectively. More details about TWUO allocation method and evaluation index of tire slip energy loss are described below.

1) TWUO Allocation Method: The TWUO CA is widely used optimization based method for vehicle stabilization, whose objective is given (Zhang and Göhlich, 2017):

$$\begin{aligned} & J = u^T \Omega u + (\chi u - \upsilon)^T \Psi (\chi u - \upsilon) \\ \text{s.t.} \quad & u_{\min} \le u \le u_{\max} \end{aligned} \tag{43}$$

where $\Omega = \mathrm{diag}\left(\frac{1}{(r_w \mu F_{z1})^2}, \frac{1}{(r_w \mu F_{z2})^2}, \frac{1}{(r_w \mu F_{z3})^2}, \frac{1}{(r_w \mu F_{z4})^2} \right)$ is the weight matrix, and Ψ is a two-dimensional diagonal penalty weight matrix to meet virtual controls. Here the SQP algorithm by Matlab library function "*fmincon*" with toleration error threshold of 0.01, is adopted for online solving of Eq. (43).

2) Tire Slip Energy Loss Calculation for Evaluation Validation: The tire slip power loss is derived from tire friction-heating dissipation on contact patch, including longitudinal power loss and lateral power loss (Zhao et al., 2019, Kobayashi et al., 2017). Through the whole cycle, the tire slip energy loss E_{total} is defined as,

$$E_{total} = E_{longitudinal} + E_{lateral} \tag{44}$$

$$\begin{cases} E_{longitudinal} = \int_0^{t_{end}} \left(\sum_{i=1}^{4} F_{xi} \kappa_i v_{xi} \cos \alpha_i \right) d\tau \\ E_{lateral} = \int_0^{t_{end}} \left(\sum_{i=1}^{4} (-F_{yi} v_{xi} \sin \alpha_i) \right) d\tau \end{cases} \tag{45}$$

where $E_{longitudinal}$ and $E_{lateral}$ denote the longitudinal tire slip energy loss and lateral tire slip energy loss, respectively. t_{end} denotes the end time instant of cycle. α_i and F_{yi} are the sideslip angle and lateral force for the i th tire, respectively.

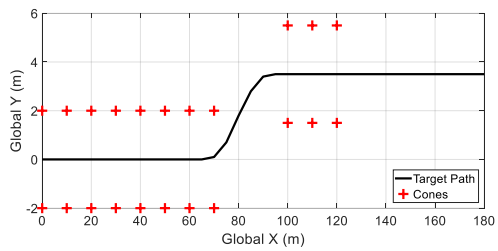

Fig. 7. SLC test cycle profile.

Table III Parameters regarding vehicle and proposed strategy.

Parameter	Value	Unit
Vehicle mass	1412	kg
Distance from CoG to front axle	1.015	m
Distance from CoG to rear axle	1.895	m
Wheel track width	1.675	m
Wheel radius	0.308	m
Vehicle rotational inertia of Z axis	1536.7	kg.m^2
Tire rotational inertia	2.5	kg.m^2
Weight matrix Q_{lqr} of LQR controller	$\mathrm{diag}([100,10^7])$	-
Weight matrix R_{lqr} of LQR controller	10^{-3}	-
Physical boundary of ΔM	±4000	N.m
Boundary of IWM torque output	±540	N.m
Predictive horizon	6	-
Sample time step in MPCA	0.01	s
Weight matrix of output state Q	$\mathrm{diag}([1,\ 1,\ 2,\ 2])$	-
Weight matrix of control increment R	$\mathrm{diag}([1000,1000,2000,2000])$	-
Weight coefficient of log function ρ	0.001	-
Allowed maximum iterative number $k_{\max}$	4	-

4.1. Control Performance Illustration

1) High Adhesion Road Test

Under this test, the target vehicle velocity and road adhesion factor are set as 80 km/h and 0.85, respectively. Fig. 8 shows the results of total traction torque, vehicle velocity, external yaw moment, and vehicle yaw rate, which yields that two methods can meet the given virtual controls and keep the yaw rate tracking error within a small range. The optimized torques by C/GMRES algorithm are illustrated in Fig. 9 and restricted within the limits of $[\tilde{u}_{\min},\tilde{u}_{\max}]$. Table IV depicts the energy loss effects of tire slip. Compared with TWUO method, the proposed method realizes the reduction of 2.34 % in tire slip power loss, where those in longitudinal and lateral directions

are 9.9 % and 0.92 %, respectively. This indicates that the proposed method is effective in saving the tire slip energy for higher utilization efficiency of vehicle power and lower tire wear.

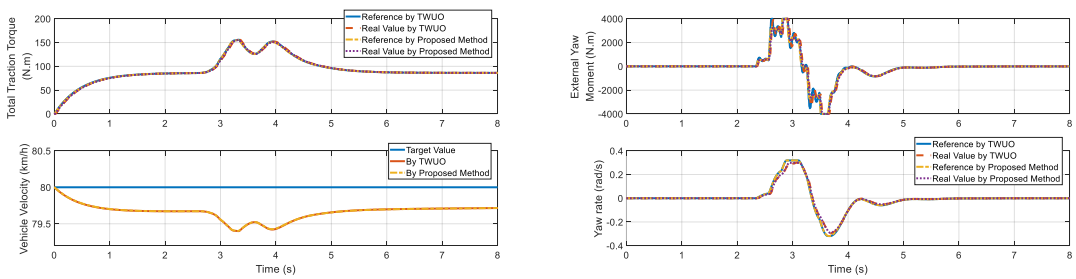

(a) (b)

Fig. 8. Virtual controls, vehicle velocity, and yaw rate under high adhesion road. (a) Total traction torque and vehicle velocity; (b) External yaw moment and yaw rate.

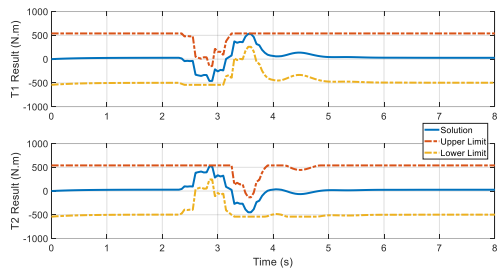

Fig. 9. Results of T_1 and T_2 by proposed method under high adhesion road.

Table IV. Tire slip power loss results under high adhesion road

Method	Longitudinal (J)	Lateral (J)	Total (J)
TWUO	1266.77	6740.70	8007.47
Proposed method	1141.36	6679.01	7820.37
Reduction (%)	9.9	0.92	2.34

To further evaluate the vehicle stability, Fig. 10 shows the results of torque allocation, tire workload usage and tire slip rate. One can find that from Fig. 10 (a), TWUO inclines to adopt the front IWMs for traction drive as much as possible. This can be explained that for the studied DDEV, owing to greater distance between CoG and rear axle, the vertical forces of rear axle are smaller than those in front axle under most of cases. According to tire adhesion circle theory (Wei et al., 2019), the rear wheels are easier to reach the tire grip margin and more sensitive to skid. Hence the greater absolute torque is arranged in front IWMs by TWUO method to reduce the total tire workload usage, as shown in Fig. 10. Instead, the MPCA allocates the IWMs' torques more evenly. From Fig. 10 (c) and Fig. 10 (d), the tire workload usages and tire slip rate by MPCA are similar with those by TWUO method. At around 2.7 s to 3.7 s, MPCA can even achieve slightly smaller tire workload usages of front wheels than TWUO method. This is because by neglecting the small $\dot{w}_i$ and considering $T_i \approx F_{xi} r_w = C_{xi} \kappa_i r_w$, the cost items in MPCA and TWUO

CA are changed to $q_i\left(v_{xi}(\tau)\kappa_i(\tau)\right)^2(C_{xi}\kappa_i)^2$ and $\left(\frac{C_{xi}\kappa_i}{\mu F_{zi}}\right)^2$, respectively. As such, at each sample instant, $F_{xi}=C_{xi}\kappa_i$ can be penalized and minimized in MPCA optimization, which plays the alike role in $\left(\frac{C_{xi}\kappa_i}{\mu F_{zi}}\right)^2$ of TWUO method. Hence that is why the CA of tire slip power loss minimization can achieve the similar tire workload usage in Fig. 10, and the quantitative results of overall tire workload usages listed in Table V also verify this viewpoint.

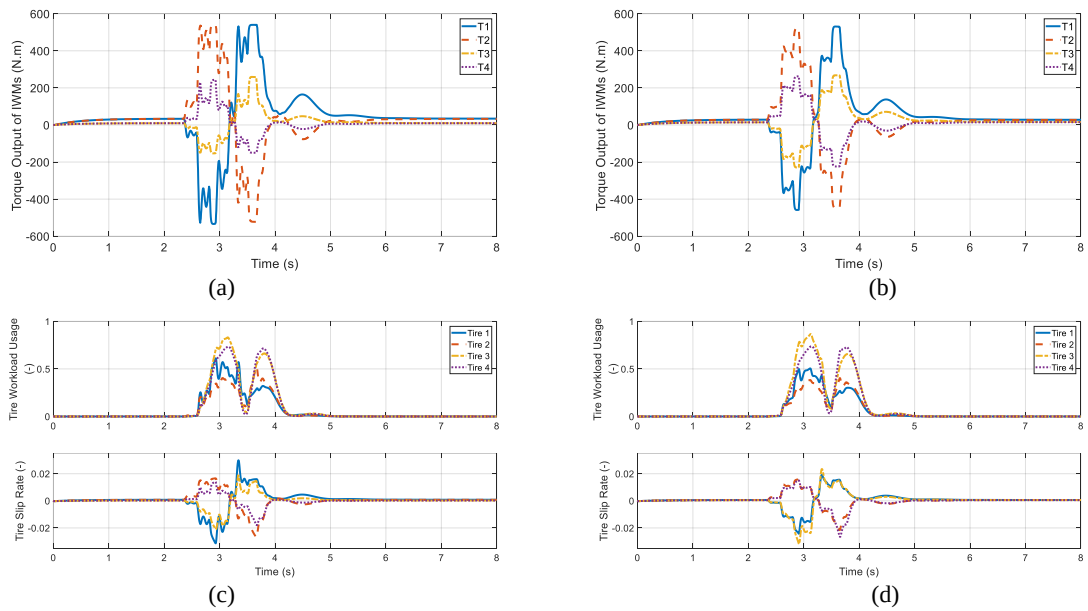

Fig. 10. Torque output, tire workload usage and tire slip rate under high adhesion road. (a) Torque output by TWUO; (b) Torque output by proposed method; (c) Tire workload usage and tire slip rate by TWUO; (d) Tire workload usage and tire slip rate by proposed method.

Table V. Overall tire workload usage under high adhesion road.

Method	Mean	Maximum	Variance
TWUO	0.2962	2.4737	0.4300
Proposed method	0.2935	2.4892	0.4205
Reduction (%)	0.88	-0.63	2.21

2) Low Adhesion Road Test

This test is conducted with target vehicle velocity of 80 km/h and adhesion factor of 0.45. Fig. 11 shows the results of virtual controls, vehicle velocity, and yaw rate. The target vehicle velocity can be effectively tracked by two CA methods, which is attributed to the guaranteed total traction torque, as shown in the top subfigure of Fig. 11 (a). From Fig. 11 (b), both allocation methods can track the yaw rate reference and target external yaw moment

within small errors, while that by MPCA yields superior transient response as drawn in the zoomed figure of Fig. 11 (b), owing to its consideration of future state trajectory in optimization.

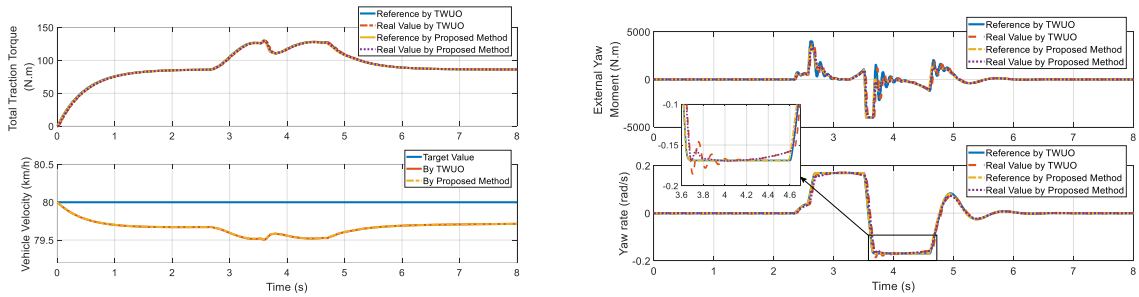

(a) (b)

Fig. 11. Virtual controls, vehicle velocity, and yaw rate under low adhesion road. (a) Total traction torque and vehicle velocity; (b) External yaw moment and yaw rate.

Fig. 12 depicts the optimized torques (i.e., T_1 and T_2) and their limits in MPCA. Compared with the results under high adhesion case, the feasible region of optimized torques is further reduced by Eq. (24) because the tire adhesion circle narrows with decreasing road adhesion factor. Even imposed by such narrow limits, the modified C/GMRES algorithm can still provide an effective solution holding the inequality constraints, as shown in the zoomed figures of Fig. 12. This also verifies the effectiveness of the propositions 1 and 2. Fig. 13 yields the accumulated tire slip energy loss results in longitudinal and lateral directions. From Fig. 13 (a), the accumulated longitudinal tire slip power variations are more like an echelon compared with that under high adhesion road, and the main tires' wear occurs during the two cornering periods of SLC cycle. From Fig. 13 (b), the accumulated lateral tire slip power loss at each tire of MPCA is nearly same with those by TWUO method. More intuitively, Table VI yields the quantificational tire slip power loss results, and the reduction of tire slip power loss by MPCA can reach 17.64 % and 1.3 % in the longitudinal and lateral directions, respectively.

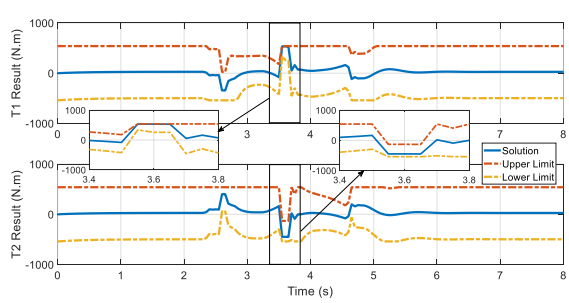

Fig. 12. Results of T_1 and T_2 by proposed method under low adhesion road.

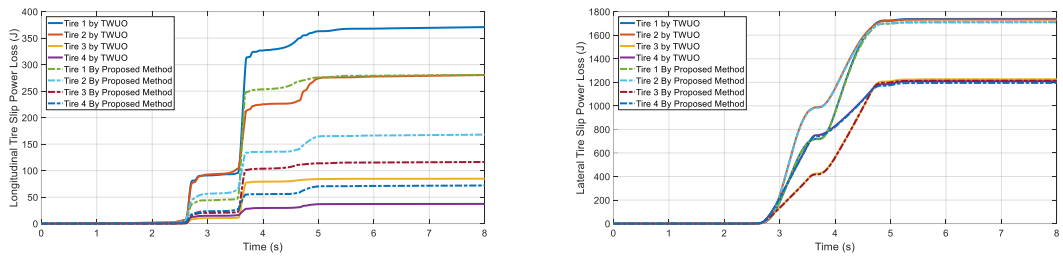

(a) (b)

Fig. 13. Accumulated tire slip power loss results by TWUO and proposed method under low adhesion road. (a) Longitudinal; (b) Lateral.

Table VI. Tire slip energy loss results under low adhesion road.

Method	Longitudinal (J)	Lateral (J)	Total (J)
TWUO	773.18	5906.66	6679.84
Proposed method	636.79	5829.67	6466.46
Reduction (%)	17.64	1.30	3.19

Fig. 14 draws the results of IWMs' torque output, tire workload usage, and tire slip rate. Unlike that under high adhesion road, the torque output of IWMs varies more sharply in this test, owing to the less feasible regions of optimization as shown in Fig. 12. From Fig. 14 (c) and Fig. 14 (d), the tire workload usage by MPCA can still be restricted below one under such a severe drive cycle. This can be explained by two reasons. First, the reference yaw rate in upper-level control is limited by $\pm 0.85\mu g / v_x$ to avoid exceeding the tire grip margin to some extent. Second, by proposed MPCA, the tire workload usage limit is constructed as an equivalent inequality constraints of Eq. (24). Given that Eq. (24) is satisfied from Fig. 12, the enlargement of tire workload usages can be restricted by proposed MPCA. For quantitative evaluation, Table VII lists the overall tire workload usage results and yields that even superior effects of tire workload usage in MPCA than TWUO method. This is caused by two reasons: 1) as mentioned in the analysis of Table V, the tire slip power loss optimization is able to minimize F_{xi} so as to reduce the tire workload usage to some extent; 2) owing to optimization of future state trajectory and the penalty item of $\left(T_i(\tau) - T_i(t_o - \Delta t)\right)$ in MPCA, the optimized torque command is smoother, which avoids the unnecessary tire workload usage.

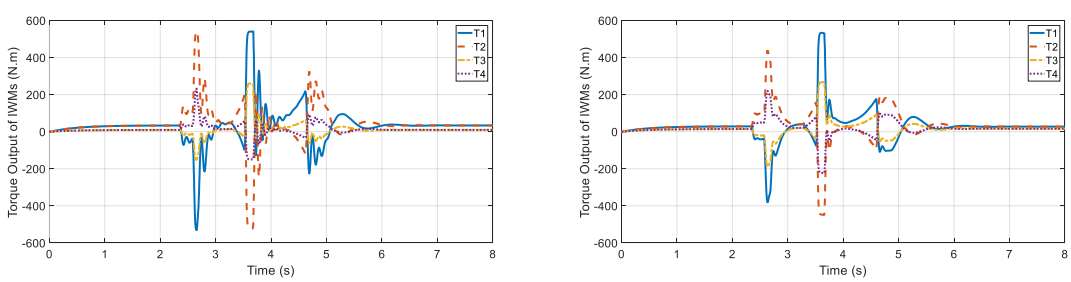

(a) (b)

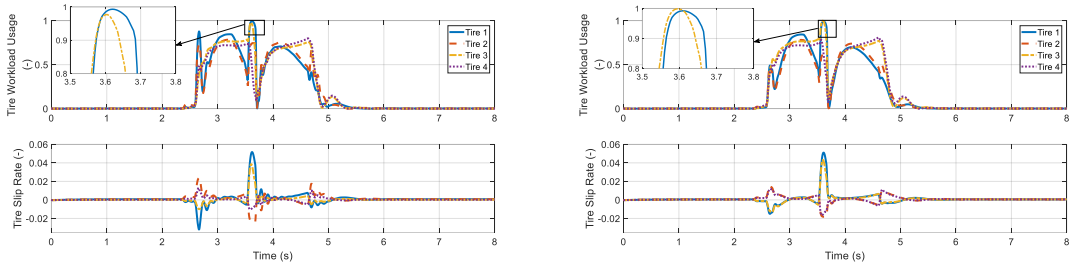

(c) (d)

Fig. 14. Torque output, tire workload usage and tire slip rate under low adhesion road. (a) Torque output by TWUO; (b) Torque output by proposed method; (c) Tire workload usage and tire slip rate by TWUO; (d) Tire workload usage and tire slip rate by proposed method.

Table VII. Overall tire workload usage under low adhesion road.

Method	Mean	Maximum	Variance
TWUO	0.7058	3.3136	1.2954
Proposed method	0.6908	3.3230	1.2678
Reduction (%)	2.1220	-0.2827	2.1270

4.2. Computational Efficiency

To validate the computational efficiency, the SQP and AS algorithms by Matlab library function "*fmincon*" with toleration error threshold of 0.01, are adopted in MPCA for comparison. Fig. 15 shows the computational time per sample in MPCAs. Compared with SQP and AS methods, the computational time per sample by C/GMRES algorithm is greatly reduced by around two orders of magnitude. Table VIII illustrates the qualified results of computational time for three algorithms. The mean and maximum calculation time by C/GMRES algorithm are much smaller than those by SQP and AS methods. Focusing on the sample step of 0.01 s in this paper, it can be concluded that among three algorithms only the C/GMRES one is real-time applicable at each sample instant in MPCA. Additionally, the variance of computational time by C/GMRES algorithm is only under the order of magnitudes of 10^{-6} and distinctly lower than those by SQP and AS algorithms, signifying the more stationary calculation time per sample in MPCA.

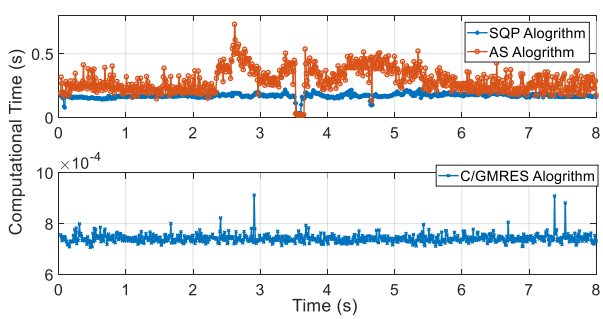

Fig. 15. Computational time illustration under high adhesion road.

Table VIII. Computational time per sample instant.

Test Cycle	Method	Mean (s)	Maximum (s)	Variance (s)
High Adhesion Road	SQP	0.1732	0.2931	0.0002
	AS	0.2994	0.7180	0.0112
	Proposed method	0.0008	0.0029	2.5×10^{-6}
Low Adhesion Road	SQP	0.1709	0.4532	0.0005
	AS	0.2901	0.7300	0.0088
	Proposed method	0.0008	0.0027	2.1×10^{-6}

V. CONCLUSION

In this paper, a fast MPCA approach is proposed in torque distribution of DDEVs to minimize tire slip power loss and guarantee vehicle stability. Here two practical assumptions are set up: 1) the vehicle acceleration and yaw rate are assumed to be measureable by GPS/INS and IMU, respectively; 2) the longitudinal velocity, road adhesion factor, and vehicle yaw rate are assumed to be "already known" by advanced estimators. To mitigate the calculation labor in MPCA, the C/GMRES algorithm is delegated for online optimization. As to reduce the calculation complexity and handle the inequality constraints, the original MPCA problem is transformed to be an unconstrained one by merging equality constraints into optimization objective and adopting external penalty method. Given this, the existence and uniqueness for solution of the modified C/GMRES algorithm are strictly proved. To extend the application of C/GMRES algorithm, a KKT optimality condition based approach is proposed for fast initialization of MPCA. The validations are carried out under two SLC tests of different tire-friction factor and yield the superior control effects by MPCA method than TWUO method in tire power loss minimization and vehicle stability. More importantly, the computational efficiency of C/GMRES algorithm is greatly higher than SQP and AS algorithms in MPCA frame. The highlighted advantages of the proposed MPCA are summed up:

1) The proposed MPCA method can effectively reduce the tire slip power loss and guarantee the vehicle stability simultaneously, which even achieves the similar tire workload usage like TWUO method does;

2) With the modifications adopted in this paper, the C/GMRES algorithm based MPCA approach can strictly satisfy the desirable equality and inequality constraints;

3) Compared with MPCAs by SQP and AS algorithms, the C/GMRES algorithm yields distinctly higher computational efficiency, indicating its potentials in real-world application.

The future work will focus on the robustness improvement of proposed MPCA due to the highly nonlinearities and uncertainties in DDEVs.

VI. ACKNOWLEDGEMENT

This work is supported by the National Natural Science Foundation of China (Grant No. 51805030) and in part by the National Natural Science Foundation of China (Grant No. 51775039). The authors would like to thank them for their support and help. In addition, the authors would also like to thank the reviewers for their corrections and helpful suggestions.

REFERENCE

ALLGOWER, E. L. & GEORG, K. 2003. Numerical Continuation Methods: An Introduction. *Mathematics of Computation,* 13**,** xxvi,388.

BOYD, VANDENBERGHE & FAYBUSOVICH 2006. Convex Optimization. *IEEE Transactions on Automatic Control,* 51**,** 1859-1859.

CHEN, Y. & WANG, J. 2014. Design and Experimental Evaluations on Energy Efficient Control Allocation Methods for Overactuated Electric Vehicles: Longitudinal Motion Case. *IEEE/ASME Transactions on Mechatronics,* 19**,** 538-548.

CORPORATION, M. S. 2019. *CarSim Information [Online]* [Online]. Available: https://www.carsim.com/products/carsim/index.php.

ENGLERT, T. & GRAICHEN, K. 2020. Nonlinear model predictive torque control and setpoint computation of induction machines for high performance applications. *Control Engineering Practice,* 99**,** 104415.

FILIPPIS, G. D., LENZO, B., SORNIOTTI, A., GRUBER, P. & NIJS, W. D. 2018. Energy-Efficient Torque-Vectoring Control of Electric Vehicles with Multiple Drivetrains. *IEEE Transactions on Vehicular Technology,* 67**,** 1-1.

GUO, H., CAO, D., CHEN, H., LV, C., WANG, H. & YANG, S. 2018. Vehicle dynamic state estimation: state of the art schemes and perspectives. *IEEE/CAA Journal of Automatica Sinica,* 5**,** 418-431.

GUO, N., LENZO, B., ZHANG, X., ZOU, Y., ZHAI, R. & ZHANG, T. 2020a. A Real-Time Nonlinear Model Predictive Controller for Yaw Motion Optimization of Distributed Drive Electric Vehicles. *IEEE Transactions on Vehicular Technology,* 69**,** 4935-4946.

GUO, N., ZHANG, X., ZOU, Y., LENZO, B. & ZHANG, T. 2020b. A Computationally Efficient Path Following Control Strategy of Autonomous Electric Vehicles with Yaw Motion Stabilization. *IEEE Transactions on Transportation Electrification***,** 1-1.

HU, C., QIN, Y., CAO, H., SONG, X., JIANG, K., RATH, J. J. & WEI, C. 2019a. Lane keeping of autonomous vehicles based on differential steering with adaptive multivariable super-twisting control. *Mechanical Systems and Signal Processing,* 125**,** 330-346.

HU, C., WANG, Z., QIN, Y., HUANG, Y., WANG, J. & WANG, R. 2019b. Lane keeping control of autonomous vehicles with prescribed performance considering the rollover prevention and input saturation. *IEEE Transactions on Intelligent Transportation Systems*.

HU, C., WANG, Z., TAGHAVIFAR, H., NA, J., QIN, Y., GUO, J. & WEI, C. 2019c. MME-EKF-based path-tracking control of autonomous vehicles considering input saturation. *IEEE Transactions on Vehicular Technology,* 68**,** 5246-5259.

JOHANSEN, T. A. & FOSSEN, T. I. 2013. Control allocation—A survey. *Automatica,* 49**,** 1087-1103.

KELLEY, C. T. 1995. *Iterative methods for linear and nonlinear equations,* Siam.

KIRK, D. E. 2004-04-30. Optimal Control Theory: An Introduction. *Dover Publications*.

KOBAYASHI, T., KATSUYAMA, E., SUGIURA, H., ONO, E. & YAMAMOTO, M. 2017. Direct yaw moment control and power consumption of in-wheel motor vehicle in steady-state turning. *Vehicle System Dynamics,* 55**,** 104-120.

KOBAYASHI, T., KATSUYAMA, E., SUGIURA, H., ONO, E. & YAMAMOTO, M. 2018. Efficient direct yaw moment control: tyre slip power loss minimisation for four-independent wheel drive vehicle. *Vehicle System Dynamics,* 56**,** 719-733.

LENZO, B., ZANCHETTA, M., SORNIOTTI, A., GRUBER, P. & NIJS, W. D. 2020. Yaw Rate and Sideslip Angle Control Through Single Input Single Output Direct Yaw Moment Control. *IEEE Transactions on Control Systems Technology***,** 1-16.

LI, B., GOODARZI, A., KHAJEPOUR, A., CHEN, S. K. & LITKOUHI, B. 2015. An optimal torque distribution control strategy for four-independent wheel drive electric vehicles. *Vehicle System Dynamics,* 53**,** 1172-1189.

MA, Y., CHEN, J., ZHU, X. & XU, Y. 2019. Lateral stability integrated with energy efficiency control for electric vehicles. *Mechanical Systems and Signal Processing,* 127**,** 1-15.

MAEDA, K., FUJIMOTO, H. & HORI, Y. Four-wheel driving-force distribution method based on driving stiffness and slip ratio estimation for electric vehicle with in-wheel motors. 2012 IEEE Vehicle Power and Propulsion Conference, 9-12 Oct. 2012 2012. 1286-1291.

NGUYEN, B.-M., HARA, S., FUJIMOTO, H. & HORI, Y. 2019. Slip control for IWM vehicles based on hierarchical LQR. *Control Engineering Practice,* 93**,** 104179.

NOCEDAL, J. & WRIGHT, S. 2006. *Numerical optimization*, Springer Science & Business Media.

OHTSUKA, T. 2004. A continuation/GMRES method for fast computation of nonlinear receding horizon control. *Automatica,* 40**,** 563-574.

PARK, G., HAN, K., NAM, K., KIM, H. & CHOI, S. B. 2020. Torque Vectoring Algorithm of Electronic-Four-Wheel Drive Vehicles for Enhancement of Cornering Performance. *IEEE Transactions on Vehicular Technology,* 69**,** 3668-3679.

POMPONI, C., SCALZI, S., PASQUALE, L., VERRELLI, C. M. & MARINO, R. 2018. Automatic motor speed reference generators for cruise and lateral control of electric vehicles with in-wheel motors. *Control Engineering Practice,* 79**,** 126-143.

QIN, Y., WANG, Z., XIANG, C., DONG, M. & WANG, R. 2018. A Novel Global Sensitivity Analysis on the Observation Accuracy of the Coupled Vehicle Model. *Vehicle System Dynamics***,** 1-22.

RAJAMANI, R. 2006. *Vehicle Dynamics and Control*, Springer Science.

SUZUKI, Y., KANO, Y. & ABE, M. 2014. A study on tyre force distribution controls for full drive-by-wire electric vehicle. *Vehicle System Dynamics,* 52**,** 235-250.

WANG, Z., QIN, Y., HU, C., DONG, M. & LI, F. 2019. Fuzzy Observer-Based Prescribed Performance Control of Vehicle Roll Behavior via Controllable Damper. *IEEE Access,* 7**,** 19471-19487.

WEI, S., ZOU, Y., ZHANG, X., ZHANG, T. & LI, X. 2019. An Integrated Longitudinal and Lateral Vehicle Following Control System With Radar and Vehicle-to-Vehicle Communication. *IEEE Transactions on Vehicular Technology,* 68**,** 1116-1127.

YOSHIMURA, M. & FUJIMOTO, H. 2012. Driving torque control method for electric vehicle with in-wheel motors. *Ieej Transactions on Industry Applications,* 181**,** 49–58.

YUAN, L., ZHAO, H., CHEN, H. & REN, B. 2016. Nonlinear MPC-based slip control for electric vehicles with vehicle safety constraints. *Mechatronics,* 38**,** 1-15.

YUE, M., YANG, L., SUN, X.-M. & XIA, W. 2018. Stability Control for FWID-EVs With Supervision Mechanism in Critical Cornering Situations. *IEEE Transactions on Vehicular Technology,* 67**,** 10387-10397.

ZHANG, X. & G HLICH, D. 2017. Improvement in the vehicle stability of distributed-drive electric vehicles based on integrated model-matching control. *Proceedings of the Institution of Mechanical Engineers Part D Journal of Automobile Engineering,* 232**,** 095440701770128.

ZHANG, X., G HLICH, D. & ZHENG, W. 2017. Karush–Kuhn–Tuckert based global optimization algorithm design for solving stability torque allocation of distributed drive electric vehicles. *Journal of the Franklin Institute,* 354**,** 8134-8155.

ZHANG, X., ZOU, Y., FAN, J. & GUO, H. 2019. Usage pattern analysis of Beijing private electric vehicles based on real-world data. *Energy,* 167**,** 1074-1085.

ZHAO, B., XU, N., CHEN, H., GUO, K. & HUANG, Y. 2019. Stability control of electric vehicles with in-wheel motors by considering tire slip energy. *Mechanical Systems and Signal Processing,* 118**,** 340-359.

ZHAO, H., REN, B., CHEN, H. & DENG, W. 2015. Model predictive control allocation for stability improvement of four-wheel drive electric vehicles in critical driving condition. *IET Control Theory & Applications,* 9**,** 2688-2696.